Proceedings of the ASME 2023 18th International Manufacturing Science and Engineering Conference
MSEC2023
June 12-16, 2023, New Brunswick, New Jersey

MSEC2023-106095

MACHINE LEARNING-BASED MODELING OF ELECTRIC-FIELD-ASSISTED DIRECT INK WRITING (EDIW) PROCESS

Yinong Chen
Department of Mechanical and Industrial Engineering, University of Illinois at Chicago, Chicago, IL

Anupam Ajit Deshpande
Department of Mechanical and Industrial Engineering, University of Illinois at Chicago, Chicago, IL

Erina Baynojir Joyee
Department of Mechanical Engineering and Engineering Science, University of North Carolina at Charlotte, Charlotte, NC

Yayue Pan
Department of Mechanical and Industrial Engineering, University of Illinois at Chicago, Chicago, IL

ABSTRACT

Direct ink writing (DIW) is an extrusion-based additive manufacturing technology. It has gained wide attentions in both industry and research because of its simple design and versatile platform. In electric-field-assisted Direct Ink Writing (eDIW) processes, an external electric field is added between the nozzle and the printing substrate to manipulate the ink-substrate wetting dynamics and therefore optimize the ink printability. eDIW was found effective in printing liquids that are typically difficult to print in the conventional DIW processes. In this paper, an eDIW process modeling system based on machine learning (ML) algorithms is developed. The system is found effective in predicting eDIW printing geometry under varied process parameter settings. Image processing approaches to collect experiment data are developed. Accuracies of different machine learning algorithms for predicting printing results and trace width are compared and discussed. The capabilities, applications and limitations of the presented machine learning-based modeling approach are presented.

Keywords: Electric-field-assisted direct ink writing (eDIW); Machine learning; Process modelling; Artificial neural network (ANN).

1. INTRODUCTION

Direct Ink Writing (DIW), also known as Robocasting, was first introduced in 1997 [1]. It is an extrusion-based layer-by-layer additive manufacturing technique that applies a constant pressure to extrude liquids or pastes along the predesigned path onto the substrate to fabricate 3D structures. Different type of materials including ceramics, polymers, metals, and composites can be used as printing ink for DIW [2-4]. DIW is one of the most versatile additive manufacturing techniques, with a wide range of applications including electronics, microfluidic devices and tissue engineering [5-7].

DIW processes can be coupled with external fields, such as magnetic, electric, or acoustic fields, to control spatial variations of microstructures of the extruded inks or even the extrusion geometry [8-10]. In particular, electric field has been found effective for not only controlling microstructures of composite inks, but also improving the printing resolution and enabling a wider range of ink choices [11-12]. Researchers have tried various ways of integrating an external electric field in DIW processes, resulting in electrohydrodynamic 3D printing, electrowetting-assisted direct ink writing, electrostatically-assisted direct ink writing processes, etc. [13-15]. In this paper, regardless of the way of integrating the electric field, we call all those systems as electric-field-assisted direct ink writing (eDIW).

In our previous works, electric field is generated near the printing orifice to change the ink flow dynamics and the extruded ink filament geometry [16-19]. By applying an external electric field, the geometry stability of the extruded ink filament can also be improved [20-21]. The present group found that the eDIW technology enabled the use of low viscosity material and broadens the choice of printable inks. In addition, the integration of electric field also enabled higher printing speed and resolution, and the use of super rough substrates.

When introducing new material to eDIW system, bulge or discontinuity issue will arise if not applying appropriate parameters during the manufacturing process [22-23]. A hybrid method based on physics and empirical parameters was

developed in our previous work for process planning [20]. The working ranges of eDIW process parameters was derived from the physic-based formulas. However, some terms involved in the calculation, like real-time contact angle and surface tension, need to be measured using complex instruments and time-consuming experimental procedures for different materials. What's more, this method is only suitable for the electrowetting-assisted DIW setup, where the electric field is added between the nozzle and substrate. Therefore, a more general modeling approach to identify the appropriate parameter settings and predict printing results need to be developed, which can be easily applied for any ink materials and any kind of eDIW setups.

As a disruptive technology widely investigated in recent years, Machine Learning (ML) has come to attention in many industries including the field of Additive Manufacturing (AM), due to its vast capabilities in data analysis such as regression and clustering [24]. ML algorithms have already demonstrated effectiveness in AM in many aspects, such as material design, in-process defect detection, quality control, geometric deviation control for manufacturing error compensation and so on [24-28]. ML algorithms also have strong ability in result prediction, after training with a set of input data. Process parameter settings can be directly used as the independent variables to train the models, which makes the process planning easy to implement.

In this paper, a ML-based system is developed to predict eDIW printing output. When developing a new material, this system can be used to research the working range of process parameter settings, to achieve a successful printed model with the target width of the printing filaments. Instead of spending large amount of time and resources to perform experiments with all combinations of parameters, this system only needs a small amount of experimental data. The system is able to predict the quality of the eDIW-printed filaments and the filament width. This prediction and modelling system can be applied to any new material using eDIW and even traditional DIW system, which can significantly save the time and labor costs when introducing new materials to the manufacturing process.

In the rest of the paper, the design of the eDIW modelling system is demonstrated in section 2. Modeling results and discussions are presented in section 3. Conclusions are drawn in section 4.

2. EDIW MODELLING SYSTEM DESIGN

2.1 Overview of Electric-field-assisted DIW Systems

Appropriate electric field settings have been found beneficial to the DIW manufacturing process, including enhanced printing speed and resolution, capability of spatially controlling fillers in ink, enabling the use of super rough substrates, etc. [16-21,29]. The electric fields can be applied in the DIW system in various ways, as shown in Figure 1. Despite the multiple ways of generating the electric field, the electric field intensity on the substrate location where the ink is deposited is used as the input parameter in the ML-based modeling approach. As a result, the proposed ML-based modeling approach can be used regardless of the way that the electric field is generated.

Here, the eDIW setup shown in Figure 1d is used to carry out experiments. Nordson EFD E3V robot is integrated with an EFD Ultimus II dispensing system, which has a pressure control accuracy of 0.1psi. A dispensing nozzle with an inner diameter of 0.4064mm was used. The standoff distance between the substrate and the nozzle was set to be 0.1mm. The electric field was generated using a custom 60-watt high voltage power source, which can provide voltage up to 30kV with a resolution of 1mV. The anode of the power source was connected to the stainless-steel dispensing nozzle. The cathode was connected to a thin copper film which was covered by 0.3mm thick double-sided polyimide (50mJ/m^2 surface energy) as the dielectric substrate on the moving platform. The distance between the dispensing nozzle and the copper sheet was calculated and the voltage was set accordingly to obtain the required electric field strength.

Parameters studied in experiments and used as input variables in the ML-based modeling system include printing speed, air pressure in the syringe, and the electric field strength.

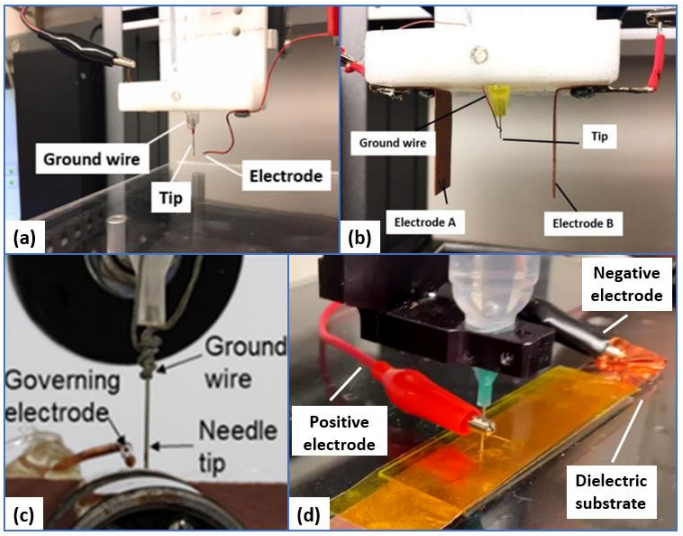

FIGURE 1: EDIW SETUP DESIGN: (A) GOVERNING ELECTRODE IN FRONT AND GROUND WIRE ON TIP [7]; (B) ELECTRIC FIELD AROUND TIP [4]; (C) GOVERNING ELECTRODE ON TOP OF BALL-BEARING [9]; (D) ELECTRODES ON TIP AND SUBSTRATE

2.2 ML-based eDIW Modeling System Design

As illustrated in Figure 2, a system for the eDIW printing output prediction is built with five steps. Starting from step 1, simple straight parallel lines are printed on the substrate with varied process parameter settings. Microscopic images of the printed samples will then be taken, which contain three to five printed lines. In step 2, the microscopic images will be processed using an VGGNetmodel to discriminate whether the sample is a

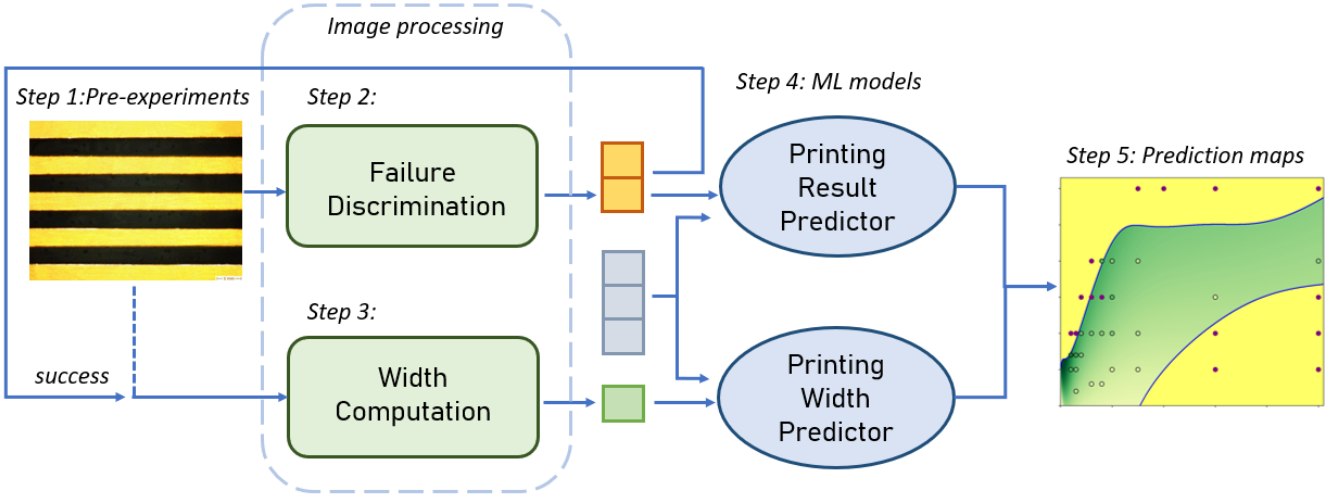

FIGURE 2: FLOW CHART OF A DATA DRIVEN PREDICTIVE MODELING SYSTEM TO PREDICT THE PRINT QUALITY AND PRINTING WIDTH

successful printing or a failed one. The average width of the printed filaments in the successfully printed samples is further computed in step 3. The collected data is used to train the ML models in step 4. After training, the ML models are used to predict the printing quality (i.e., success or failure) and filament width under varied process parameter settings.

2.3 Preliminary Experiments

A new DIW ink material developed in our previous study is used as a test case here to show the ML-based modelling approach [21]. Specifically, 1 wt.% Poly(3,4-ethylenedioxythiophene):polystyrene sulfonate (PEDOT:PSS) dispersion (CLEVIOS™, PH 1000) was purchased from Heraeus, Germany. Poly(ethylene oxide) (PEO) particles (Mw~10000, Sigma Aldrich, Germany) was mixed with the PEDOT:PSS dispersion to prepare the mixture. PEO powder was added in a ratio of 52 wt.%, calculated based on solid weight of PEO and PEDOT:PSS. All materials were used as received. The mixture was stirred in a magnetic stirrer at 200 rpm for 17 hours before use. Three levels of electric field strength, 0kV/cm, 4kV/cm, and 8kV/cm were studied over printing speed values ranging from 20mm/s to 500mm/s and air pressure values ranging from 0.2psi to 3psi.

As listed in Table 1, ten groups of experiments were designed with different levels of three process parameters, i.e., controllable factors A, B, and C. Two replicates were conducted. In total, 252 tests were performed by printing 5 parallel straight lines under the specified parameter setting. After ink drying, the printed samples were characterized by taking microscopic images. For example, Figure 3 shows microscopic images of four printed samples. The yellow background is the substrate, and the black color is the printed ink. The microscopic images will then be analyzed in step 2 as detailed in the following section.

Process input parameters (factors)	(A) Pritning speed (mm/s)	(B) Air pressure (psi)	(C) Electric field strength (kV/cm)
Group 1	20	0.2/0.5/0.7/1	0/4/8
Group 2	30	0.2/0.5/0.7/1	0/4/8
Group 3	40	0.3/0.7/1/1.5	0/4/8
Group 4	60	0.3/1/1.5/2	0/4/8
Group 5	80	0.3/1/1.5/2	0/4/8
Group 6	100	0.5/1/1.5/2	0/4/8
Group 7	150	0.5/1/2/3	0/4/8
Group 8	200	1/1.5/2/3	0/4/8
Group 9	300	0.5/1/1.5/2/3	0/4/8
Group 10	500	0.5/1/1.5/2/3	0/4/8

TABLE 1: PRELIMINARY EXPERIMENTS DESIGN

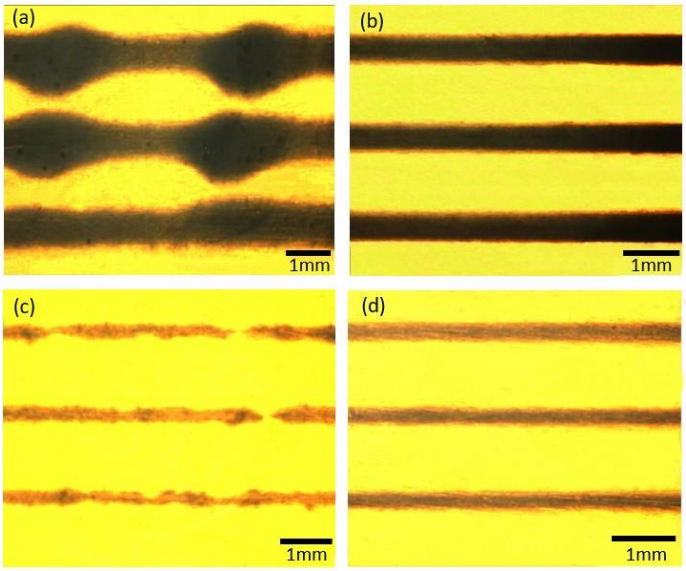

FIGURE 3: (A) BULGE SAMPLE; (B) BULGE ISSUE SOLVED BY ADDING 8KV/CM ELETRIC FIELD; (C) DISCONTINOUS SAMPLE; (D) DISCONTINOUS ISSUE SOLVED BY ADDING 8KV/CM ELETRIC FIELD.

2.4.1 Image-based Failure Discrimination

Common defects and failures in eDIW include bulge and discontinuity as shown in Figure 3a and 3c, respectively. Due to the relatively large width of the printed lines, classical line detection methods such as Probabilistic Hough Transform (PHT) does not work well for processing the microscopic images. Another route may be training or fine-tuning deep learning networks, but it is not suitable for small dataset. To analyze the microscopic images of the printed samples and detect printing failures, here we investigated texture classification method, which is a robust yet faster method.

In particular, Leung-Malik (LM) filter bank [30], a multi-scale, multi-orientation filter bank with 48 different filters is used here. The filters are hand-crafted with arbitrary kernel sizes as (49,49) in the experiments. The LM filter bank has a total of 48 filters, 2 Gaussian derivative filters at 6 orientations and 3 scales, 8 Laplacian of Gaussian filters and 4 Gaussian filters. There are two filters particularly sensitive to shape change in vertical direction and best suit the needs for detections of bulge or discontinuity in the printed samples.

Given the specific filters with the kernel size, we can use it to conduct 2D convolution on any given image. the images were first converted to grayscale images in which the substrate is white color and the ink is black. The grayscale conversion reduces the number of channels from 3 to 1. The convolution is done on a GPU with the deep learning platform PyTorch. The program classifies any images with identified pixels above a certain threshold as failure and classify as success otherwise. By carefully tuning the threshold, an accuracy up to 96.8% can be achieved for detecting images with printing failures. However, this method was time consuming, and the threshold need to be adjusted manually for every group of experiment setting. Therefore, another method, VGGNet (Figure 4) was used to generate a computer vision classifier, to automatically identify images of failure samples.

60% of the pre-experiment images were randomly chosen as training data while the rest was set as testing data. The training data were used to train VGGNet. Pytorch was used to extract the features of the images, transferring the images from 480×640×3 to 1×4096 vectors. Those vectors were used as the input data for the deep learning neural network. After fitting a linear classification model, we got the result as a 2×4096 matrix, adding the linear classifier result (i.e., class 1: failure, or class 2: success). The cross-entropy loss functions were used to optimize the training model. We found that the best result was given when setting the batch size as 32. Then this well-trained system was able to identify the existing of bulge and the discontinuous part shown on the pre-experiment images, achieving an accuracy as high as 94%.

2.4.2 Printing Width Computation

For images detected as success from the previous step, the average widths of printed lines were computed. Here, the canny algorithm [31] was used to extract the successfully printed line structure, after the success images were converted to grayscale. The "higher and lower sensitivity thresholds" were turned to 400 and 700, respectively. However, Canny algorithm is not able to distinguish the upper and lower boundaries of printed filaments,

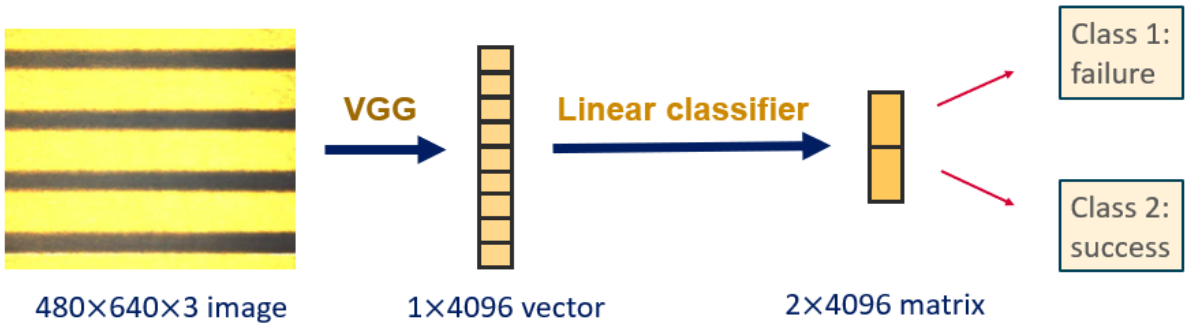

FIGURE 4: VGG NEURAL NETWORK SYSTEM FOR FAILURE RESULT DETECTION

which means, all identified lines structures were displayed in yellow color in the canny map (Figure 5b).

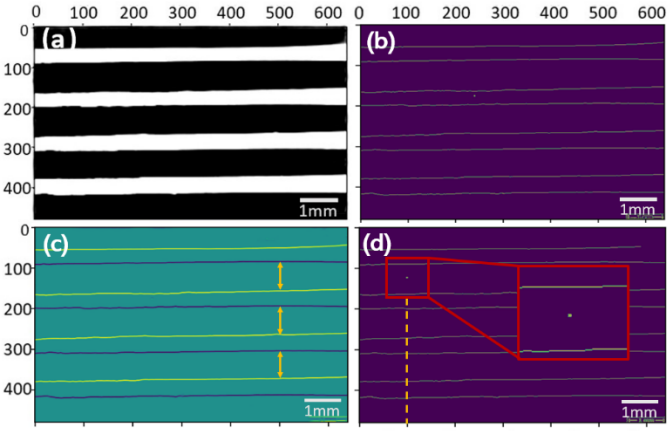

FIGURE 5: WIDTH MEASUREMENT PROCESS: (A) GREYSCALE IMAGE; (B) APPLY CANNY ALGORITHM TO GREYSCALE IMAGE; (C) APPLY SOBEL FILTER TO GREYSCALE IMAGE; (D) CANNY MAP WITH NOISE ON FIRST DETECTING COLUMN.

To handle the scenario where lines are close to the top or bottom edges of the images and are not complete in the image, Sobel filter [32] was added to compute the pixel gradient change direction of each detected edge, to see whether it changes from black pixel to white or from white pixel to black. Positive pixel derivative (i.e., black to white) indicates the lower boundary while negative pixel derivative stands for upper boundary. If the image begins with a lower boundary or ends with an upper boundary, the line would be detected as incomplete and would be dropped. Figure 5 is an example of the width measurement process. After applying Canny algorithm to a grayscale image (Fig.5a), the edges were extracted and highlighted (Fig.5b). Next step was transforming the grayscale image to a Sobel algorithm map, where the upper boundary is detected as deep blue color and the lower boundary as yellow color (Fig.5c). In this example, the first printed line was not counted into later calculation since the first boundary was not in deep blue. Similarly, the last filament was also dropped because of the lack of lower boundary. The printed lines that can be counted in further steps are indicated by orange arrows in Figure 5c.

Five detection points at the pixel column of 100, 200, 300, 400 and 500 among the 640 pixels in x direction were defined to compute the average width. The width of the printed filaments was measured as the distance between the neighboring upper and lower boundaries in detection columns. The positions of pixels in x and y direction obtained from Canny algorithm, and the pixel derivatives gotten from Sobel algorithm, were used to compute the distance. An average width was calculated using the line widths at all detection columns. It is possible to have noise on the detection column, which could seriously affect the result. An example is shown in Figure 5d, noise exists on the first detection column, which exists on the original images or is generated in image transform process. To address this challenge, we added some checking code to remove the effect of noise. If an odd number of points was detected in a detection column, then this detection column would be discarded and only the results obtained from the other four detection columns would be used to calculate the average width. If in one detection column, the width of any filament is more than 15 pixels larger than others, then this detection column will also be considered to have noise and be discarded.

3. RESULTS AND DISCUSSION

3.1 Printing Result Prediction

The printing speed, air pressure and electric field strength settings were collected and used as independent variables for the machine learning model training. The printing result (e.g., success or failure) of the pre-experiment samples, which are determined in VGG model in image processing step, were treated as dependent data to train the machine learning model. The data collected for pre-experiments were randomly split into two sets, i.e., 60% as training data and 40% as testing data. Several different classification models were investigated to fit the training data, including logistic regression, Support Vector Machines (SVM) with different functions, random forest, and Multi-Layer Perceptron (MLP) classifier.

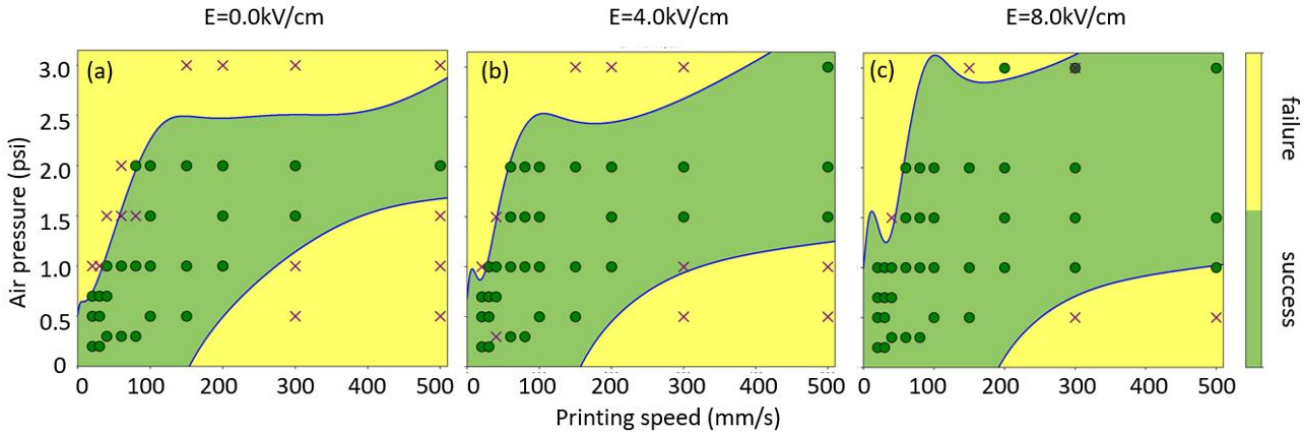

FIGURE 6: PRINTING RESULT PREDICTION FROM MLP CLASSIFIER MODEL

The prediction of printing result is a 2-class classification problem. Logistic regression model is one of the simplest algorithms which generates a decision boundary between two classes. The model predicts the probability of occurrence of two classes and gives the predicted classification according to the probability. SVM algorithm generates hyperplanes as decision boundaries to classify the data points in high dimensional feature space. SVM finds an optimal hyperplane with the maximum margin, which means the hyperplane has the maximum distance between training data points in two classes. To train SVM models, we have investigated linear function, radial basis functions and polynomial functions with different degrees and regularization weights as kernel functions of the hyperplane.

Instead of generating boundaries between two classes to make the prediction, random forest model provides a decision analysis method to solve the classification problem. In this approach, multiply decision trees were created, where the conjunctions of the features are represented by the branches of trees. The final prediction of the random forest is related to the selection of most decision trees. It is also possible to draw decision boundaries based on the output of random forest model. However, even though the accuracy of boundary can be improved by adding the number of decision trees, the boundary lines are still not as smooth as the other algorithms. Compared to traditional machine learning approaches, neural network models have bigger expressive compacity. MLP is one of the most commonly used feedforward Artificial Neural Network (ANN) model. MLP classifier consists of more than three layers of nodes, which are fully connected to the following layer. The input data sets are mapped to the output predictions through the nonlinear activation functions of the nodes of the layers.

The testing results of different functions were summarized and compared in Table 2.

Machine learning models	Testing accuracy
Logistic regression	80.47%
SVM (linear function kernel)	78.09%
SVM (radial basis function kernel)	81.27%
SVM (4-degree polynomial function kernel)	76.57%
Random forest (n=200)	98.01%
MLP Classifier	94.62%

TABLE 2: TESTING ACCURACY FOR THE PRINTING QUALITY PREDICTION

From Table 2, it can be seen that the random forest gives the highest accuracy (i.e., 0.98). However, due to its inherent principle, random forest model can't provide a smooth boundary for the printing result prediction. Therefore, the MLP classifier which gives an accuracy of 94.62% and a smooth boundary is considered as the best choice.

The decision boundaries of the two classes predicted by MLP are shown in Figure 6, where the results are listed for different electric field strength (0, 4, 8 kV/cm). The yellow area is failure where printing result would have bulge or discontinuity problems, and the green area is success where ink can be successfully deposited and solidified on the substrate without defects. Normally, the top left yellow area is failure with bulge observed on printed lines. The bottom right yellow area is failure where printed lines break to segments. The points represent the experiment data. Dark green points represent the successfully printed experiments and the purple crosses represent the failure experiments. It was found that the MLP classifier model produced the smoothest boundary among all the tested models. The boundary line for the top left part is kind of up and down because the resolution of the air pressure is limited (i.e., only 0.1psi) and the input data is also limited in this region. The weight percentage of the failure points is increased to generate a clear boundary. These results also show that the printable area is significantly increased with the increase of the electric field strength, which indicates the enhancement of printability by incorporating the electric field. This prediction is consistent with the experimental findings concluded in our previous work [20].

3.2 Printing Width Prediction

To predict the printed line width, the input data (independent variables) are printing speed, air pressure, and electric field strength, while the output data (dependent variable) is the average width computed from step 3, the width computation step. The data set are randomly split into 60% as training data and the remaining 40% as testing.

Here, polynomial regression models with degrees ranging from 1 to 5 were investigated. The performance fails to meet the expectation probably because of the over-fit issue. Therefore, ridge regression models are introduced here to apply L2 regularization to the polynomial functions which suffered from multicollinearity. Besides, MLP regressor, decision tree and random forest model with 2000 benches were also investigated to fit the data and predict the printing width. Two criteria were used to evaluate the training score of the models, mean squared error and coefficient of determination. The smaller the mean squared error and the larger the coefficient of determination, the better the training result. The scores were listed in Table 3.

Compared with all other models, random forest gives the smallest mean squared error and the largest coefficient of determination. The prediction results for the printing speed in range of 0-500 mm/s and air pressure from 0 to 3.0 psi under 0/4/8kV/cm electric field were shown in Figure 7 a-c, combined with the printable boundaries obtained from printing result prediction. However, an unavoidable problem generated by using random forest method was that the resolution of the prediction is strongly relying on the parameter intervals in the pre-experiments. It provides high accuracy prediction for the testing data, which have the same interval of parameters as training data. However, when the random forest model is used to predict the printing width using input variables with a smaller interval, the predicting score is not good anymore. Same problem occurs with decision tree model.

Machine learning models		Mean squared error	Coefficient of determination
Polynomial regression	1 degree	0.025387	0.1493
	2 degrees	0.007963	0.7332
	3 degrees	0.004779	0.8399
	4 degrees	0.028729	0.0373
	5 degrees	0.003737	0.8748
Ridge regression	2 degrees (alpha=0.1)	0.008026	0.7311
	3 degrees (alpha=0.01)	0.004773	0.8401
	4 degrees (alpha =0.01)	0.003539	0.8814
	5 degrees (alpha =0.01)	0.003844	0.8712
MLP Regressor		0.003177	0.8935
Decision Tree		0.003437	0.8848
Random Forest (n=2000)		0.001218	0.9592

TABLE 3: TESTING SCORE FOR PRINTING WIDTH PREDICTION

MLP regressor model (Figure 7 d-f) is again found to work best among all methods, as it showed smooth and high score prediction. With the MLP regressor model, it is possible to predict the printing result in high resolution without narrow down the input parameter interval. It means that we can use a small amount of pre-experiment data to develop a high-fidelity model to predict the printing results and printing width of the eDIW process under varied process settings. When increasing air pressure or decreasing printing speed, the printing width rises because of the enlarged volume of material. The printing width also grows with the increase of the applied electric field strength, which agrees well with the physical explanation. When a larger electric field strength is applied, the contact angle between extruded ink and substrate reduces and hence the line width increases.

Combining the outcome obtained from printing result and printing width predictions, the final prediction maps is established in Fig. 7. To summarize, to develop a printing prediction map for a new ink, a small set of preliminary experiments (less than 300 tests) needs to be conducted to collect experimental data to train the models. The amount of experimental data needed depends on the range of parameters to study. Printed samples are then characterized by microscopic imaging. Experimental data including printing results (success or failure) and printing width of the successfully-printed samples are extracted from imaging processing and then used to train ML models. In this study, MLP method was found to be the most effective ML model and was chosen to generate the prediction map. After training, the MLP model-based prediction system is able to predict the printing result and printing width for any process parameter settings within the range, which can be used for eDIW process planning.

4. CONCLUSION

In summary, an ML-based modeling approach is developed to predict the eDIW printing result and guide the eDIW process planning. This modeling approach can be applied to any inks and any electric field configurations without barriers, promoting the development and utilization of new materials for eDIW and facilitating eDIW process planning for any printing tasks.

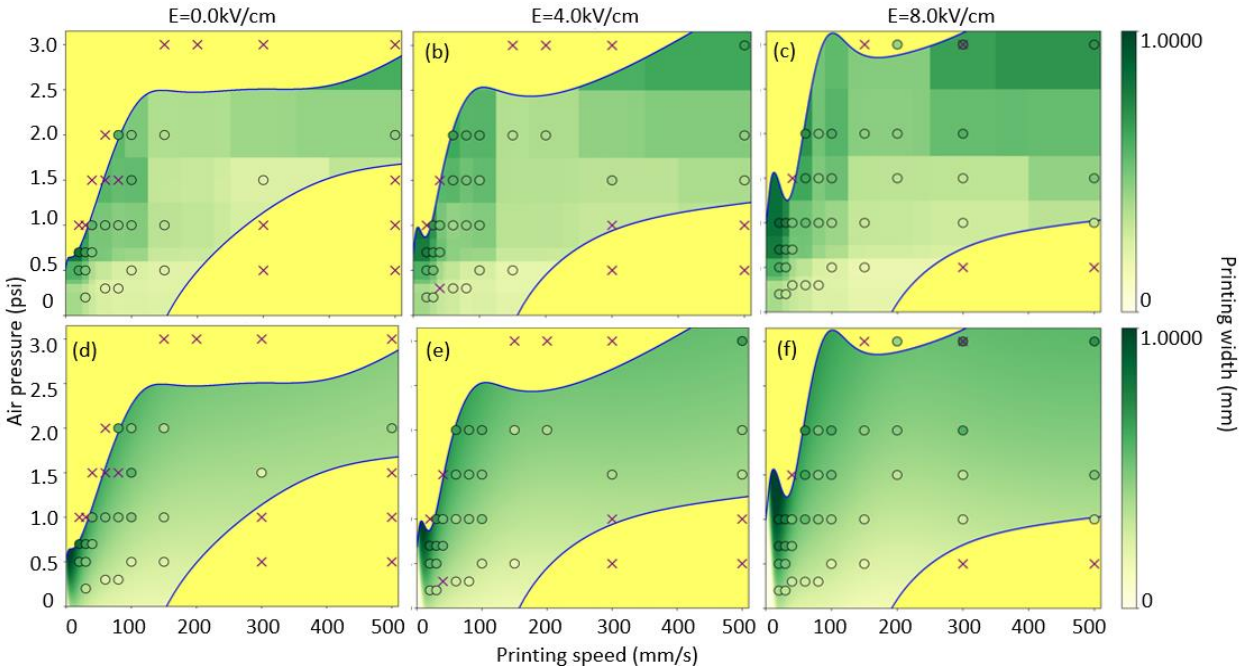

FIGURE 7: PRINTING WIDTH PREDICTION FROM RANDOM FOREST MODEL (A-C) AND MLP REGRESSOR (D-F).

ACKNOWLEDGEMENTS

This project was partially supported by National Science Foundation (NSF) Grant 1825626.

REFERENCES

[1] Cesarano TIl, Joseph, Thomas A. Baer, and Paul Calvert. "Recent developments in freeform fabrication of dense ceramics from slurry deposition." *1997 International Solid Freeform Fabrication Symposium. 1997.*

[2] Lewis, Jennifer A., et al. "Direct ink writing of three-dimensional ceramic structures." *Journal of the American Ceramic Society* 89.12 (2006): 3599-3609.

[3] Neumann, Taylor V., and Michael D. Dickey. "Liquid metal direct write and 3D printing: a review." *Advanced Materials Technologies* 5.9 (2020): 2000070.

[4] Saadi, M. A. S. R., et al. "Direct Ink Writing: A 3D Printing Technology for Diverse Materials." *Advanced Materials* (2022): 2108855.

[5] Sun, Ke, et al. "3D printing of interdigitated Li‐Ion microbattery architectures." *Advanced materials* 25.33 (2013): 4539-4543.

[6] Therriault, Daniel, Scott R. White, and Jennifer A. Lewis. "Chaotic mixing in three-dimensional microvascular networks fabricated by direct-write assembly." *Nature materials* 2.4 (2003): 265-271.

[7] Ma, Yue, et al. "Three‐dimensional printing biotechnology for the regeneration of the tooth and tooth‐supporting tissues." *Biotechnology and Bioengineering* 116.2 (2019): 452-468.

[8] Friedrich, Leanne, et al. "Acoustic control of microstructures during direct ink writing of two-phase materials." *Sensors and Actuators A: Physical* 268 (2017): 213-221.

[9] Kokkinis, Dimitri, Manuel Schaffner, and André R. Studart. "Multimaterial magnetically assisted 3D printing of composite materials." *Nature communications* 6.1 (2015): 1-10.

[10] Korukunda, Tulja Bhavani, et al. "Enhanced infiltration and morphology of bismuth perovskite in Carbon-stack solar cells–A synergistic effect of electric fields in modified spray technique." *Solar Energy* 241 (2022): 386-395.

[11] Chen, Jianzhou, et al. "Fabrication of flexible organic electronic microcircuit pattern using near-field electrohydrodynamic direct-writing method." *Journal of Materials Science: Materials in Electronics* 30.19 (2019): 17863-17871.

[12] Huang, Yanhua, Yang Cao, and Hantang Qin. "Electric Field Assisted Direct Writing and 3D Printing of Low‐Melting Alloy." *Advanced Engineering Materials* (2022): 2200091.

[13] Jiang, Jiaxin, et al. "Electrohydrodynamic direct-writing micropatterns with assisted airflow." *Micromachines* 9.9 (2018): 456.

[14] Watson, Alexander M., Alexander B. Cook, and Christopher E. Tabor. "Electrowetting‐assisted selective printing of liquid metal." *Advanced Engineering Materials* 21.10 (2019): 1900397.

[15] Ramos, Pierre G., et al. "Enhanced photoelectrochemical performance and photocatalytic activity of ZnO/TiO2 nanostructures fabricated by an electrostatically modified electrospinning." *Applied Surface Science* 426 (2017): 844-851.

[16] Plog, Jevon, et al. " Electrostatic charging and deflection of droplets for drop-on-demand 3D printing within confinements" *Additive Manufacturing* (2020): 101400

[17] Jiang, Yizhou, et al. "Direct ink writing of wearable thermoresponsive supercapacitors with rGO/CNT composite electrodes." Advanced Materials Technologies 4.12 (2019): 1900691.

[18] Plog, J., et al. "Control of direct written ink droplets using electrowetting." Langmuir 35.34 (2019): 11023-11036.

[19] Plog, Jevon, et al. "Electrostatically-assisted direct ink writing for additive manufacturing." *Additive Manufacturing* 39 (2021): 101644.

[20] Jiang, Yizhou, et al. "Electrowetting-assisted direct ink writing for low-viscosity liquids." Journal of Manufacturing Processes 69 (2021): 173-180.

[21] Wang, Xinnian, et al. "3D PRINTING OF HIGHLY CONDUCTIVE PEDOT: PSS-BASED POLYMERS." *Journal of Manufacturing Science and Engineering* (2022): 1-25.

[22] Romberg, Stian K., et al. "Linking thermoset ink rheology to the stability of 3D-printed structures." *Additive Manufacturing* 37 (2021): 101621.

[23] Ma, Siqi, et al. "Direct ink writing of geopolymer with high spatial resolution and tunable mechanical properties." *Additive Manufacturing* 46 (2021): 102202.

[24] Wang, Chengcheng, et al. "Machine learning in additive manufacturing: State-of-the-art and perspectives." Additive Manufacturing 36 (2020): 101538.

[25] Meng, Lingbin, et al. "Machine learning in additive manufacturing: a review." Jom 72.6 (2020): 2363-2377.

[26] Roach, Devin J., et al. "Utilizing computer vision and artificial intelligence algorithms to predict and design the mechanical compression response of direct ink write 3D printed foam replacement structures." *Additive Manufacturing* 41 (2021): 101950.

[27] Zhang, Haining, and Seung Ki Moon. "Reviews on machine learning approaches for process optimization in noncontact direct ink writing." *ACS Applied Materials & Interfaces* 13.45 (2021): 53323-53345.

[28] Johnson, N. S., et al. "Invited review: Machine learning for materials developments in metals additive manufacturing." *Additive Manufacturing* 36 (2020): 101641.

[29] Liashenko, Ievgenii, Joan Rosell-Llompart, and Andreu Cabot. "Ultrafast 3D printing with submicrometer features using electrostatic jet deflection." *Nature communications* 11.1 (2020): 1-9.

[30] Malik TLaJ. Representing and recognizing the visual appearance of materials using three-dimensional textons. *International Journal of Computer Vision.* 2001 Jun;43(1):29–44.

[31] Canny, John. "A computational approach to edge detection." *IEEE Transactions on pattern analysis and machine intelligence* 6 (1986): 679-698.
[32] G. A. Ramirez. (2009, April) sobel.cpp. [Online]. Available: http://www.cs.utep.edu/ofuentes/AI/sobel.cpp.